Journal of Alloys and Compounds 509 (2011) 2434–2440

Contents lists available at ScienceDirect

Journal of Alloys and Compounds

journal homepage: www.elsevier.com/locate/jallcom

Enhanced photoelectrocatalytic degradation of 2,4-dichlorophenoxyacetic acid by $CuInS_2$ nanoparticles deposition onto TiO_2 nanotube arrays

Ronghua Liu[a], Yutang Liu[a,b], Chengbin Liu[a,*], Shenglian Luo[a,c,*], Yarong Teng[a], Lixia Yang[a,c], Renbin Yang[b], Qingyun Cai[a]

[a] State Key Laboratory of Chemo/Biosensing and Chemometrics, Hunan University, Changsha 410082, People's Republic of China
[b] College of Bioscience and Biotechnology, Hunan Agricultural University, Changsha 410128, People's Republic of China
[c] School of Environment and Chemical Engineering, Nanchang Hangkong University, Nanchang, 330063, People's Republic of China

ARTICLE INFO

Article history:
Received 20 July 2010
Received in revised form 3 November 2010
Accepted 4 November 2010
Available online 13 November 2010

Keywords:
TiO_2 nanotube
$CuInS_2$
Photoelectrocatalysis
2,4-Dichlorophenoxyacetic acid

ABSTRACT

Surface modification of TiO_2 nanotube (NT) arrays with $CuInS_2$ nanoparticles (NPs) for photocatalytic degradation of 2,4-dichlorophenoxyacetic acid (2,4-D) was reported. A pulse electrodeposition technique was used to prepare the $CuInS_2$ NPs, and the resulted $CuInS_2$ NPs, with a uniform size of about 20 nm, were found to deposit on the top surface of the highly oriented TiO_2 NT while without clogging the tube entrances. Compared with the unmodified TiO_2 NT, the $CuInS_2$ NPs modified TiO_2 NT ($CuInS_2$–TiO_2 NT) showed significantly enhanced photocatalytic activity towards 2,4-D under visible light. After 160 min irradiation, the removal rate of 2,4-D is 100% by using $CuInS_2$–TiO_2 NT, much higher than 65.2% by using the unmodified TiO_2 NT in photoelectrocatalytic process. The increased photodegradation efficiency mainly results from the improved photocurrent density as results of enhanced visible-light absorption and decreased hole-electron recombination due to the presence of narrow-band-gap p-type semiconductor $CuInS_2$.

1. Introduction

The photocatalytic degradation of pollutants using titanium dioxide (TiO_2) has been extensively studied for environmental protection [1–5], and it is still the most promising photocatalyst because of its exceptional properties such as high efficiency, low cost, chemical inertness, and photostability. However, the widespread technological use of TiO_2 is retarded by its wide band gap (3.0 eV for the rutile and 3.2 eV for the anatase phases), which requires ultraviolet irradiation that accounts for only 4–5% of the spectrum of solar energy for photocatalytic activation. Additionally, the efficiency of photocatalytic degradation is limited by the high recombination rate of the photogenerated electron–hole pairs. Quite a few different methods have been developed to increase the photocatalytic efficiency of TiO_2, such as doping TiO_2 with transition metal cations [6,7] or nonmetal anions [8–10] to enhance the visible light absorbance, and modifying TiO_2 with noble metals [11,12] or semiconductors [13,14] to improve the separation and transport of photocarriers during photocatalysis.

The ternary I–III–VI_2 chalcopyrites are important in solar energy materials, and especially, the semiconductor $CuInS_2$ shows industrial potential in photovoltaics because of its high absorption coefficient and direct band gap of 1.52 eV which lies in the optimum range for solar energy conversion [15,16]. In this respect, $CuInS_2$ is expected to be a promising material for photocatalysis. However, to our best knowledge, there is one report about $CuInS_2$ thin films on TiO_2/FTO glass substrates for photovoltaic application [17], and another report on the photocatalytic activity of the $CuInS_2$–TiO_2 composites where TiO_2 nanopartciles were used as the photocatalyst [18]. Compared with TiO_2 powders, TiO_2 nanotube arrays, grown from a titanium sheet by electrochemical anodic oxidation, have a highly ordered structure, large specific surface area, and fast electron transport. Further, the combination of $CuInS_2$ and TiO_2 NT arrays will make the composites more practical and cost-effective because of its simple preparation and separation compared to the powdery TiO_2 photocatalyst.

$CuInS_2$ can be prepared by many techniques [19–24]. Among them, electrodeposition technique is more attractive due to its simplicity and low cost. Single step direct electrodeposition to prepare $CuInS_2$ thin films has been reported by many researchers [25,26]. Recently, a pulsed electrodeposition technique, based on a multipulse sequence of current densities or potentials of equal amplitude and duration, has been proposed for the preparation of metal or metal oxide nanocrystals [27,28]. By this technique, nucleation and growth of the crystallites can be controlled by

* Corresponding authors at: State Key Laboratory of Chemo/Biosensing and Chemometrics, Hunan University, Changsha 410082, People's Republic of China. Tel.: +86 731 88823805.
E-mail addresses: chem_cbliu@hnu.cn, chem_cbliu@163.com (C. Liu), sllou@hnu.cn (S. Luo).

0925-8388/$ – see front matter © 2010 Elsevier B.V. All rights reserved.
doi:10.1016/j.jallcom.2010.11.040

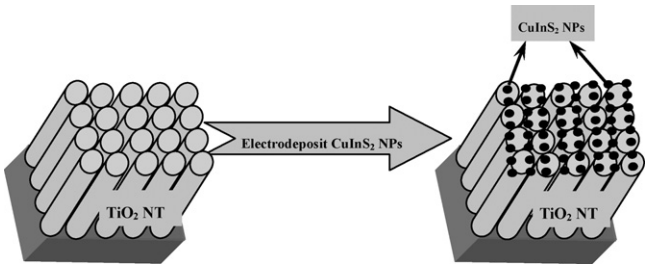

Scheme 1. Schematic diagram showing the fabrication process of $CuInS_2$–TiO_2 NT arrays.

varying the pulse amplitude and duration, and thus, it is helpful to obtain monodisperse nanostructured materials. In this work, the $CuInS_2$ nanoparticles were deposited using pulse potential deposition onto TiO_2 NT ($CuInS_2$–TiO_2 NT), and we investigated the photocatalysis of the $CuInS_2$–TiO_2 NT composites towards 2,4-dichlorophenoxyacetic acid (2,4-D) in detail. 2,4-D, a model pollutant, has drawn considerable attention in photocatalytic degradation recently, considering that it is a typical widely used and highly toxic synthetic phytohormone.

2. Experimental

2.1. Chemicals and materials

Titanium foil (99.8%, 250 μm thickness) was purchased from Aldrich (Milwaukee, WI), 2,4-dichlorophenoxyacetic acid (2,4-D) was obtained from Shanghai Chemical Corporation of China. All other reagents were of the highest commercially available quality and purified before use. Deionized water was used for preparation of all aqueous solutions.

2.2. Preparation of TiO_2 nanotube arrays

TiO_2 NT arrays were prepared according to our previous work [29]. Prior to anodization, titanium ribbons (4 cm × 1 cm) were ultrasonically cleaned in acetone and ethanol, respectively. The cleaned titanium ribbon was anodized at 15 V in an electrolyte containing 0.1 M NaF and 0.5 M $NaHSO_4$ at 25 °C for 5 h using a two-electrode system with a platinum cathode where the distance between the two electrodes was 2 cm, resulting in the TiO_2 NT arrays with a pore size of 90–100 nm, a length of 320 nm and an efficient electrode area of 3 cm × 1 cm on each side.

2.3. Preparation of $CuInS_2$ modified TiO_2 NT arrays by pulse electrodeposition

A typical three-electrode electrochemical cell was equipped with a Pt wire as the counter electrode, a saturated calomel electrode (SCE) as the reference electrode and a TiO_2 NT arrays as the working electrode. The electrolyte solution contained $CuC1_2$ (2 mM), $InCl_3$ (2 mM) and $Na_2S_2O_3$ (20 mM) (Cu:In:S = 1:1:10). Pulsed potentials were applied to the cathode, where the "on" potential was −2.5 V vs. SCE, the "off" potential was −0.000001 V vs. SCE, the "on" time was 0.5 s, and the "off" time was 1.0 s. The loading amount of the deposit can be tuned by adjusting the number of pulse sequence, and here 300 and 600 pulse sequences were chosen for deposition (Scheme 1). After deposition, the $CuInS_2$ modified TiO_2 NT was washed several times with distilled water, and then heated in nitrogen atmosphere at 500 °C for 3 h.

2.4. Characterization of TiO_2 NT arrays

The morphologies of the unmodified and modified TiO_2 NT were investigated by using a field emission scanning electron microscope (FESEM, Hitachi, model S-4800). Energy dispersive X-ray (EDX) spectrometers fitted to electron microscopes were used for elemental analysis. The crystal phases of the resulting TiO_2 arrays were determined by an X-ray diffractometer with Cu-K_α radiation (XRD, M21X, MAC Science Ltd., Japan). Photoluminescence (PL) spectra were recorded using Hitachi F-2500 fluorescence spectrophotometer at an excitation wavelength of 270 nm.

2.5. Optical and electrochemical measurements

The absorption spectra were recorded by using the UV–vis diffuse reflectance spectra (Cary 300, USA) equipped with an integrating sphere in radius of 150 mm. Photoelectrochemical investigation was carried out in a three-electrode configuration with TiO_2 NT arrays or $CuInS_2$–TiO_2 NT arrays as the working electrode, a Pt foil as the counter electrode and a saturated calomel electrode (SCE) as the reference in a 0.05 M Na_2SO_4 or 1 M KOH solution as the electrolyte. Illuminated current was recorded by an electrochemical working station (CH Instruments, model CHI 660B). A 500 W xenon arc lamp (CHF-XQ-500W, Beijing Changtuo Co. Ltd.) served as the visible light source (280–2000 nm) with the excitation density of 100 mW cm^{-2} measured by NOVA Oriel 70260 with a thermodetector.

2.6. Photoelectrocatalytic degradation of 2,4-D

The catalytic degradation experiments were carried out in a quartzose beaker. The unmodified or modified TiO_2 NT arrays as the working electrode were placed in a beaker with a platinum electrode as the counter electrode and a saturated calomel electrode as the reference. All the experiments were performed in a 60 mL aqueous solution containing Na_2SO_4 (0.05 M) and 2,4-D (10 mg L^{-1}), where the pH of the solution was 3.0 unless otherwise stated. The variation of 2,4-D concentration was traced by an UV–vis spectrophotometer based on its characteristic absorbance values at 227 nm. At least triplicate runs were carried out for each test, and the standard deviation was generally less than 10%.

3. Results and discussion

3.1. Morphology of the $CuInS_2$–TiO_2 NT arrays

The surface morphologies of the samples characterized by SEM are shown in Fig. 1. The electrochemical anodization of a titanium sheet produced high-density, well-ordered, and uniform TiO_2 NT arrays with the tube diameters ranging from 90 to 100 nm and the wall thickness of 5 nm (Fig. 1a). The formation mechanism of the TiO_2 NT has been well documented previously [29,30]. After pulse potential deposition, more $CuInS_2$ nanoparticles were efficiently deposited onto the top surface of the highly oriented TiO_2 NT arrays than those onto the inner surface of the tubes (Fig. 1b). When the pulse sequence was increased from 300 to 600, significant increase of the particle density was observed (Fig. 1c). In the following, the $CuInS_2$–TiO_2 NT arrays prepared under 300 and 600 pulse sequences were named as 300-$CuInS_2$–TiO_2 NT and 600-$CuInS_2$–TiO_2 NT, respectively. In both cases, the $CuInS_2$ NPs are uniform with a similar size of about 20 nm, and the ultra-fine-grained structures minimize the clogging at the tube entrances. As a consequence, the maximum distribution of $CuInS_2$ nanoparticles on the top surface of the tubes without pore clogging is favorable for light absorption. The composition of the samples was determined by EDX spectroscopy, and the EDX result shows that the modified TiO_2 NT contains the elements of O, Cu, In, S, and Ti (Fig. 1d). The calculated molar percentages of Cu, In and S are about 0.12%, 0.11% and 0.23%, respectively, corresponding to the molar ratio of 1:1:2.

3.2. XRD spectra analysis

The XRD spectra of both the unmodified TiO_2 NT (Fig. 2a) and the $CuInS_2$–TiO_2 NT (Fig. 2b) exhibit the characteristic diffraction peaks of anatase phase at 25.49°, 38.56°, 48.14° and 54.10° corresponding to the lattice distance of 3.50, 2.34, 1.89 and 1.70 Å, respectively. Compared with the unmodified TiO_2 NT, $CuInS_2$–TiO_2 NT shows two additional peaks at 27.90° and 46.35° with the corresponding lattice constant values of 3.20 and 1.96 Å, indicating the existence of the tetragonal-phase crystalline $CuInS_2$ NPs.

3.3. DRS spectra analysis

The UV–vis diffuse reflectance spectra of the samples are shown in Fig. 3. There are two characteristic absorption peaks of TiO_2. The first one at about 380 nm results from the absorption of the trapped hole, and the other one at around 470–600 nm is due to the absorption of the trapped electron at the Ti^{4+} center [31]. Compared with the unmodified TiO_2 NT, $CuInS_2$–TiO_2 NT has stronger absorption in the visible region and produces a red-shift absorption edge from about 550 to 720 nm due to $CuInS_2$ with a narrow band gap responsible for the improved absorption capability of TiO_2 NT in the visible light region. Owing to the increased loading of $CuInS_2$ NPs, the 600-

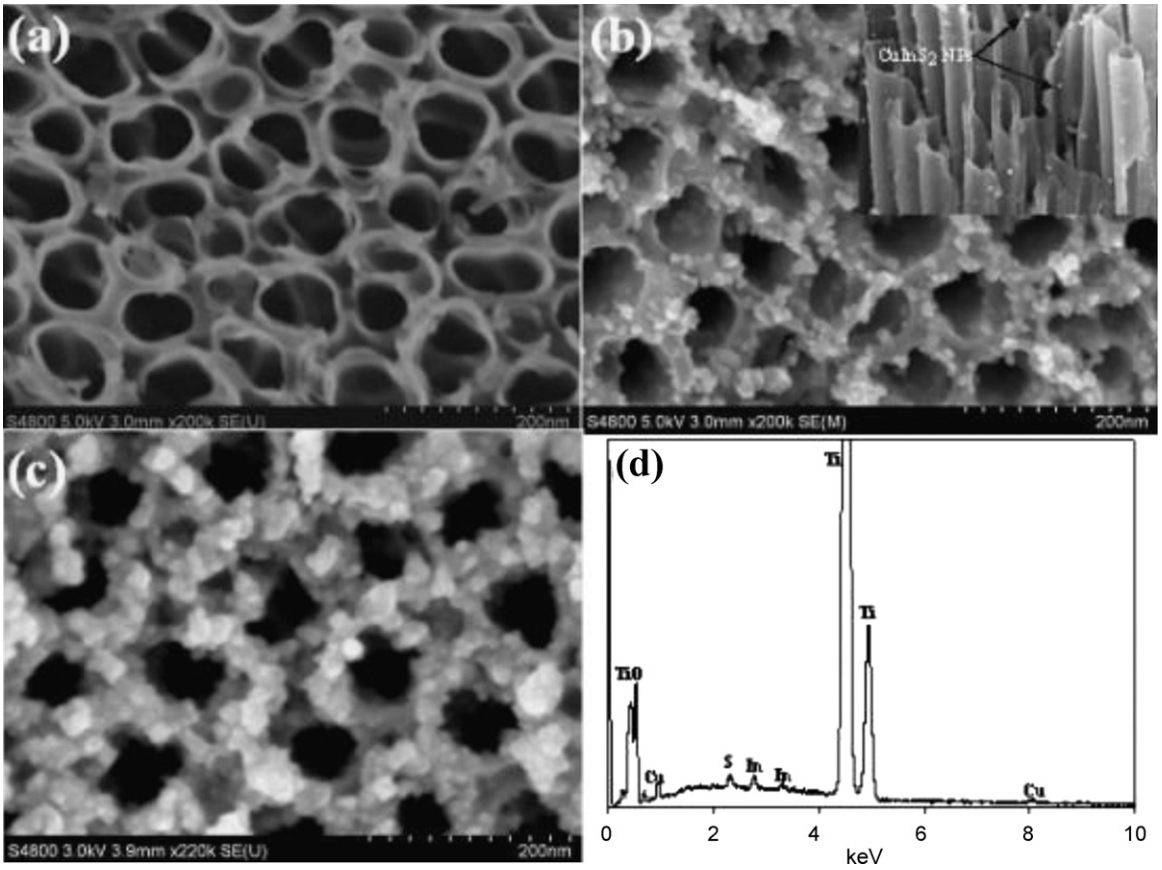

Fig. 1. Top-surface SEM images of (a) unmodified TiO_2 NT, $CuInS_2$ nanoparticles modified TiO_2 NT with pulse sequences of (b) 300 and (c) 600, and (d) EDX pattern of the specimen shown in panel (b). The inset in panel (b) is a corresponding cross-sectional SEM image.

$CuInS_2$–TiO_2 NT produced an increased absorption in the visible light region compared with the 300-$CuInS_2$–TiO_2 NT.

3.4. Photoelectrochemical properties of the $CuInS_2$–TiO_2 NT arrays

The photoelectrochemical response of the samples was analyzed under visible light with the measured density of 100 mW cm^{-2}. The curves shown in Fig. 4 were collected from TiO_2 NT and $CuInS_2$–TiO_2 NT in a 0.05 M Na_2SO_4 solution. The dark currents of both TiO_2 NT and $CuInS_2$–TiO_2 NT are always near zero. The photocurrent densities of 600-$CuInS_2$–TiO_2 NT and 300-$CuInS_2$–TiO_2 NT are 1.95 mA cm^{-2} and 2.94 mA cm^{-2}, over 2 and 3 times larger than that of the TiO_2 NT (0.82 mA cm^{-2}), respectively. This reflects the higher separation efficiency of photo-induced electrons and holes in the case of $CuInS_2$–TiO_2 NT composites. Although 600-$CuInS_2$–TiO_2 NT has stronger UV–vis absorption compared to the 300-$CuInS_2$–TiO_2 NT, its photocurrent density is lower, which is probably due to a larger amount of $CuInS_2$ nanoparticles on

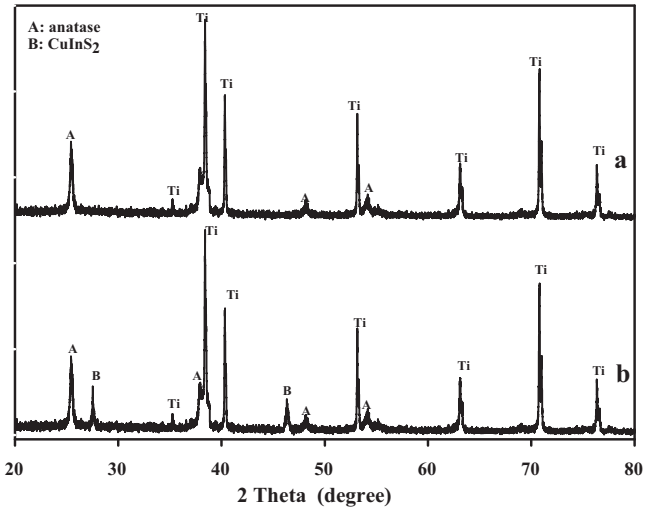

Fig. 2. XRD patterns of (a) unmodified TiO_2 NT and (b) $CuInS_2$–TiO_2 NT.

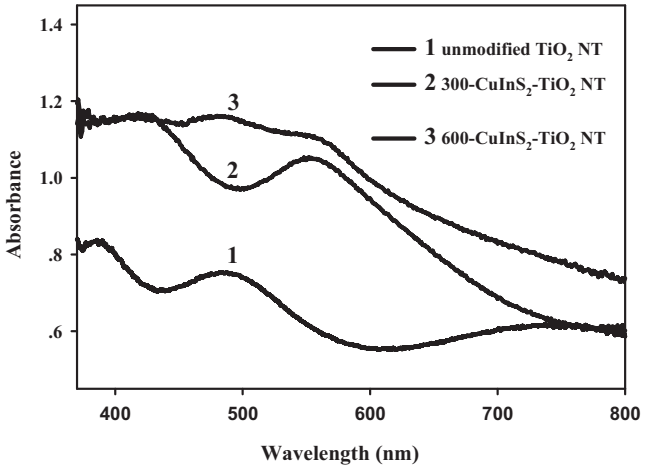

Fig. 3. UV–vis diffuse reflectance spectra of unmodified TiO_2 NT and $CuInS_2$–TiO_2 NT under 300 or 600 pulse sequences.

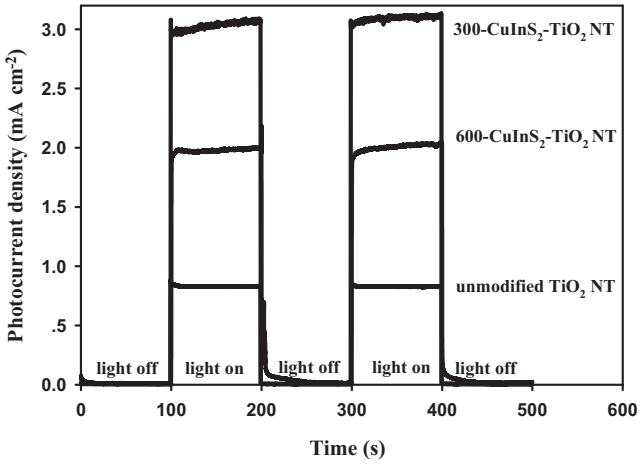

Fig. 4. Photocurrent response of unmodified TiO_2 NT and $CuInS_2$–TiO_2 NT under 300 or 600 pulse sequences in 0.05 M Na_2SO_4 solution.

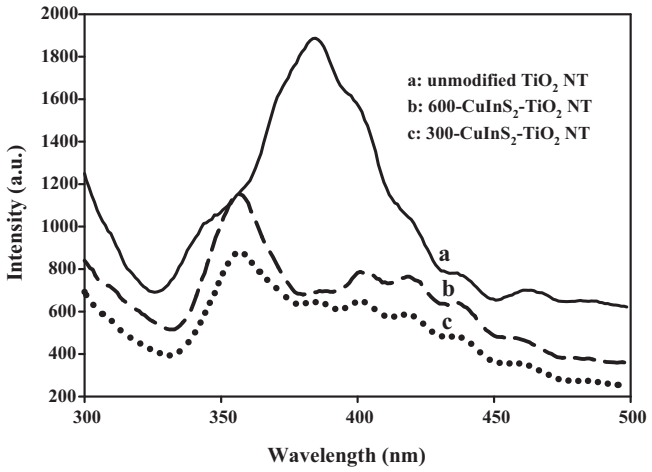

Fig. 6. PL spectra of unmodified TiO_2 NT and $CuInS_2$–TiO_2 NT under 300 or 600 pulse sequences. The excitation wavelength is 270 nm.

the surface of the TiO_2 NT arrays hindering the light absorption of TiO_2 NT itself and the effective transfer of the photogenerated charges. Therefore, 300-$CuInS_2$–TiO_2 NT is expected to exhibit the minimal recombination of photogenerated charges during photocatalysis and to be a good photocatalyst for organic pollutant degradation.

3.5. Current–voltage characterization

To further study the photoelectric properties of the samples, current–voltage (*I–V*) characteristics of all the samples were characterized in 1 M KOH electrolyte. Consistent with the results of Fig. 4, the dark current of TiO_2 NT is near zero, while upon illumination, all the TiO_2 NT samples show increased photocurrent densities with increasing the potentials (Fig. 5). As expected, the photocurrent densities of the $CuInS_2$–TiO_2 NT arrays electrodes are much higher than that of the TiO_2 NT electrode. Similarly, the photocurrent of the 600-$CuInS_2$–TiO_2 NT is lower than that of 300-$CuInS_2$–TiO_2 NT. Meanwhile, as we can see from the Fig. 5, the modification of $CuInS_2$ results in a negative shift of the zero-current potential from −0.6 to −0.75 V (or −0.79 V), further confirming that the $CuInS_2$ can enhance the separation of the photo-generated electrons and holes of TiO_2 NT [32].

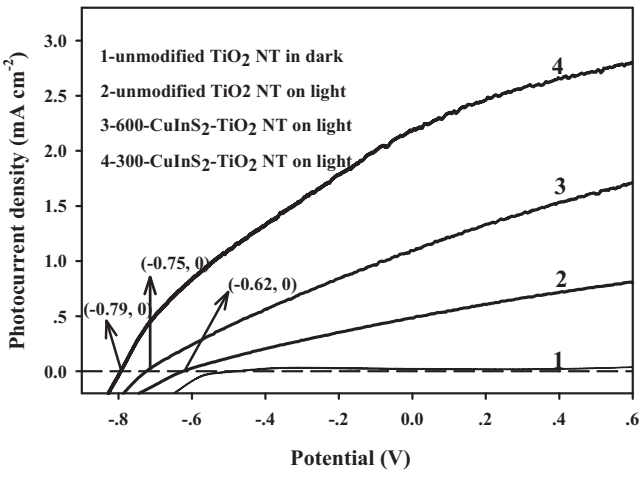

Fig. 5. Current–voltage characteristics for unmodified TiO_2 NT and $CuInS_2$–TiO_2 NT under 300 or 600 pulse sequences in 1 M KOH solution.

3.6. Photoluminescence spectra analysis

The photoluminescence emission spectra have been widely used to investigate the efficiency of charge carrier trapping, immigration and transfer, and to understand the fate of electron–hole pairs in semiconductor particles [33]. In Fig. 6, the modified and unmodified TiO_2 NT arrays exhibit similar broad PL emission bands, whereas the PL intensity decreases in the order of unmodified TiO_2 NT < 600-$CuInS_2$–TiO_2 NT < 300-$CuInS_2$–TiO_2 NT. This implies that the presence of $CuInS_2$ NPs reduces the possibility of the electron–hole recombination, especially for the TiO_2 NT modified with $CuInS_2$ NPs under 300 pulse sequences.

3.7. Photoelectrocatalytic degradation 2,4-D

Degradation of 2,4-D was performed through electrochemical (EC) process without light irradiation, direct photolytic (DP) process without catalyst, photocatalytic (PC) process, and photoelectrocatalytic (PEC) process. For light irradiation, a 500 W xenon arc lamp with the excitation density of 100 mW cm^{-2} was used as the light source (280–2000 nm). 2,4-D removal efficiency was calculated by the following formula:

$$2,4\text{-D removal efficiency} = \left[\frac{C_0 - C_t}{C_0}\right] \times 100\%$$

where C_0 is the initial 2,4-D concentration and C_t is the 2,4-D concentration obtained after various intervals of time.

As shown in Fig. 7, both the EC degradation of 2,4-D on $CuInS_2$–TiO_2 NT and the DP degradation of 2,4-D without catalyst exhibit very low degradation efficiency, while the degradation efficiencies significantly improved in the PC and PEC processes. The PEC degradation efficiencies of 2,4-D with a bias potential (0.5 V vs. SCE) are higher than those in PC cases, because the applied bias potential makes more efficient separation of photo-producing electron–hole pairs. After being degraded for 160 min, the removal rate of 2,4-D is 100% by using $CuInS_2$–TiO_2 NT, much higher than 65.2% by using the unmodified TiO_2 NT in the PEC process, and 93.4% of 2,4-D by using $CuInS_2$–TiO_2 NT, much higher than 54.9% by using the unmodified TiO_2 NT in the PC process, respectively. The results indicate that light irradiation is crucial for $CuInS_2$ TiO_2 NT to degrade 2,4-D, and the $CuInS_2$–TiO_2 NT is more effective than the unmodified TiO_2 NT arrays for photocatalysis.

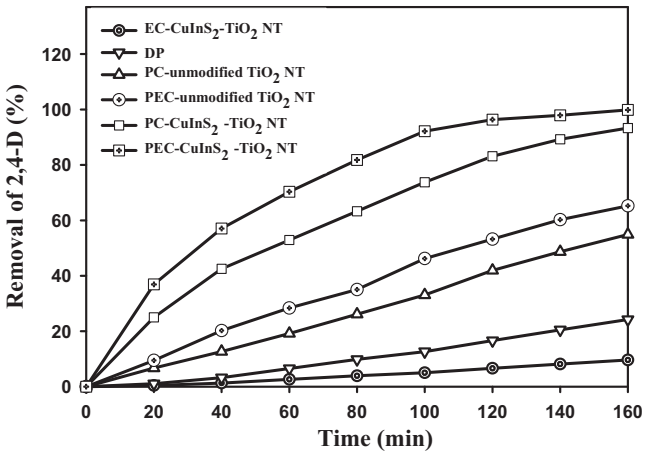

Fig. 7. The curves obtained from electrochemical (EC), direct photolytic (DP), photocatalytic (PC) and photoelectrocatalytic (PEC) degradation of 2,4-D on different catalysts. The initial concentration of 2,4-D was 10 mg L^{-1} and the pH value was 3.

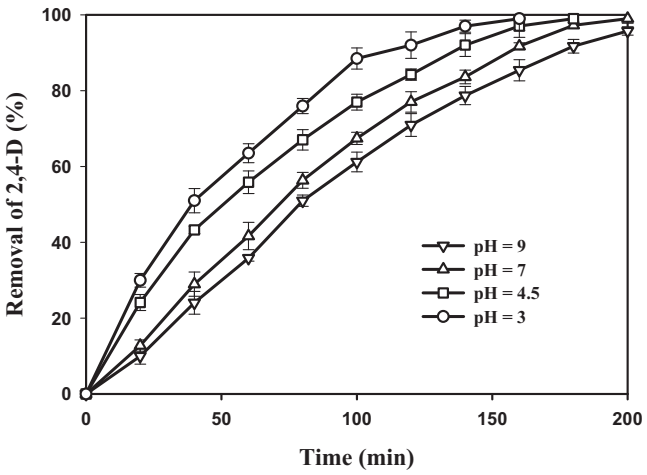

Fig. 8. The effect of pH on the removal of 2,4-D with degradation time in PEC process. The initial concentration of 2,4-D is 10 mg L^{-1}.

The photocatalytic reaction kinetics follows the Langmuir–Hinshelwood model:

$$r = -\frac{dC}{dt} = \frac{k_r K_a C}{(1 + K_a C)}$$

where k_r and K_a represent rate constant and adsorption constant, respectively. The equation can be simplified to an apparent first-order equation [34,35]

$$\ln\left(\frac{C_0}{C}\right) = k_r K_a t = kt$$

where C, C_0, and k represent the concentration of 2,4-D at a certain time (t), the initial concentration of 2,4-D, and the first-order rate constant, respectively. The values of kinetic constants (k) of 2,4-D photodegradation in different processes are listed in Table 1, and the corresponding linear regression coefficients (R) are also listed, which indicates a good linear relationship.

3.8. Factors affecting PEC degradation of 2,4-D

As we know, the PEC behaviors of photocatalysts are sensitive to pH value [36–38] and electrolyte concentration [39,40]. Herein, we investigated the effects of pH and electrolyte concentration on the PEC degradation of 2,4-D using $CuInS_2$–TiO_2 NT arrays catalyst.

3.8.1. pH effect

Fig. 8 shows the removal efficiency of 2,4-D vs. the degradation time at different pH values during PEC process. 100%, 96.5%, 82.3%, and 75.6% of 2,4-D were removed in 160 min at pH = 3, 4.5, 7, and 9, respectively. The results demonstrated that 2,4-D was degraded faster in acidic solution than in alkaline solution. Similar phenomena were also observed from the electrochemical assisted photocatalytic degradation of other organic pollutants [36,37]. The effect of pH value could be described as Eqs. (1)–(11) [37]:

$$TiO_2 \xrightarrow{h\nu} e^- + h^+ \quad (1)$$

$$h^+ + H_2O \rightarrow {}^\bullet OH + H^+ \quad (2)$$

$$OH^- + h^+ \rightarrow {}^\bullet OH \quad (3)$$

$$e^- + O_2 \rightarrow {}^\bullet O_2^- \quad (4)$$

$${}^\bullet O_2 + H^+ \rightleftharpoons HO_2^\bullet \quad pKa = 4.88 \quad (5)$$

$$2HO_2^\bullet \rightarrow O_2 + H_2O_2 \quad (6)$$

$$HO_2^\bullet + {}^\bullet O_2^- \rightarrow HO_2^- + O_2 \quad (7)$$

$$HO_2^- + H^+ \rightarrow H_2O_2 \quad (8)$$

$$H_2O_2 + e^- \rightarrow {}^\bullet H_2O_2 \quad (9)$$

$${}^\bullet H_2O_2 + {}^\bullet O_2^- \rightarrow {}^\bullet OH + OH^- + O_2 \quad (10)$$

$$H_2O_2 \xrightarrow{h\nu} 2{}^\bullet OH \quad (11)$$

When pH value is higher than 4.88 pKa for producing $HO_2^\bullet$ free radicals, the reaction will proceed in the reverse direction. The lack of $HO_2^\bullet$ free radicals makes Eqs. (6)–(11) difficult to proceed. Therefore, the formation of •OH free radicals was supplied by the reaction of positive holes with water and OH^- on the surface of titanium dioxide [38]. For pH value lower than 4.88 in Eq. (5), the reaction favors the formation of $^\bullet HO_2$ to support reaction (6) and the following ones for producing more •OH free radicals. The kinetic constants of 2,4-D degradation at different pH values and the corresponding linear regression coefficients (R) are shown in Table 2.

3.8.2. Electrolyte concentration

In order to maximize the degradation rate of target pollutants and minimize the formation of toxic intermediates, electrolyte concentration plays a very important role in PEC process, because some anions of the electrolyte may participate in the degradation

Table 1
The values of rate constant (k) and regression coefficients (R) of 2,4-D photoelectrocatalytic degradation with different processes.

Processes	Rate constant, k (min^{-1})	R^2
PEC ($CuInS_2$–TiO_2 NT)	0.1011	0.9642
PC ($CuInS_2$–TiO_2 NT)	0.0660	0.9754
PEC (Unmodified TiO_2 NT)	0.02865	0.9871
PC (Unmodified TiO_2 NT)	0.0200	0.9811
DP	0.0149	0.9969
EC ($CuInS_2$–TiO_2 NT)	0.0121	0.9912

Table 2
The values of rate constant (k) and regression coefficients (R) of 2,4-D degradation in PEC process at different pH values.

pH	Rate constant, k (min^{-1})	R^2
3	0.1011	0.9642
4.5	0.0860	0.9754
7	0.0626	0.9811
9	0.0542	0.9878

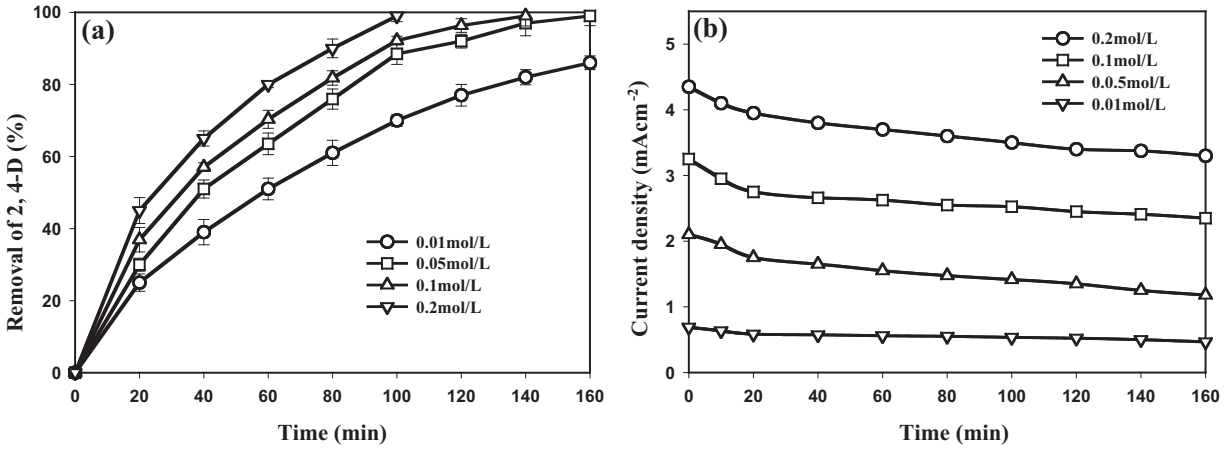

Fig. 9. (a) The effect of Na_2SO_4 concentrations (0.01, 0.05, 0.1, and 0.2 M) on the removal of 2,4-D and (b) the current density during PEC process. The initial concentration of 2,4-D is 10 mg L^{-1}, the potential is 0.5 V and the pH value was 3.

reaction of target pollutants [39,40]. Sodium chloride may electrochemically convert to chlorine, which may further react with target pollutants (or its intermediates) to produce polychlorinated compounds [36]. When sulfate was used as electrolyte, the degradation rate of target pollutant increased with increasing electrolyte concentration because of increased electrical conductivity and the formation of peroxysulfate anions [37,40]. It is obvious that both the degradation rate of 2,4-D (Fig. 9a) and the current density (Fig. 9b) enhance with increased Na_2SO_4 concentration. Moreover, the current density reaches their maximum value at the initial reaction time and then it gradually minishes with the reaction proceeding. This is also a reason why the removal rate is higher in the beginning of the PEC process.

3.9. Photocatalytic mechanism discussion

Scheme 2 illustrates the transfer processes of photogenerated electrons and holes in the catalytic system of $CuInS_2$–TiO_2 NT. As is well known, $CuInS_2$ is a p-type semiconductor, and its combination with TiO_2 leads to the formation of p–n junction [18,41]. Herein, when $CuInS_2$ NPs were deposited onto the surface of the TiO_2 NT, a p–n junction was formed between them. Under simulated solar light irradiation, electrons of $CuInS_2$ NPs and TiO_2 NT were excited by visible and UV light, respectively, from the valence band (VB) to the conduction band (CB). The photogenerated electrons of $CuInS_2$ CB move to the TiO_2 CB and the photogenerated holes of TiO_2 VB move to the $CuInS_2$ VB, hindering their recombination that usually occurs in the unmodified TiO_2. The electrons of TiO_2 coupled with the electrons captured from $CuInS_2$ were shuttled freely along the oriented TiO_2 NT driven by the bias voltage, giving rise to larger photocurrent in $CuInS_2$–TiO_2 NT composites than in unmodified TiO_2 NT. In the case of photodegradation experiments, more •OH free radicals were formed by the chemical reactions of electrons so that an enhanced degradation efficiency was obtained on the $CuInS_2$–TiO_2 NT composites. On the other hand, if the loading amount of $CuInS_2$ NPs is beyond the critical value, UV light rays arriving at the surface of TiO_2 NT will be weakened, leading to decreased amount of the photogenerated electrons in TiO_2 NT, and low photocurrent density (see, for example, the 300-$CuInS_2$–TiO_2 NT and 600-$CuInS_2$–TiO_2 NT in Figs. 4 and 5)

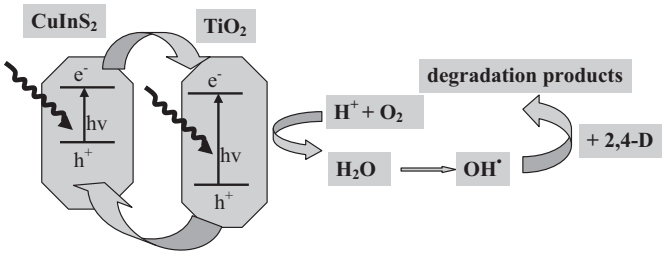

Scheme 2. Illustration of the electron and hole transfer in $CuInS_2$–TiO_2 NT and the mechanism of photocatalysis degradation.

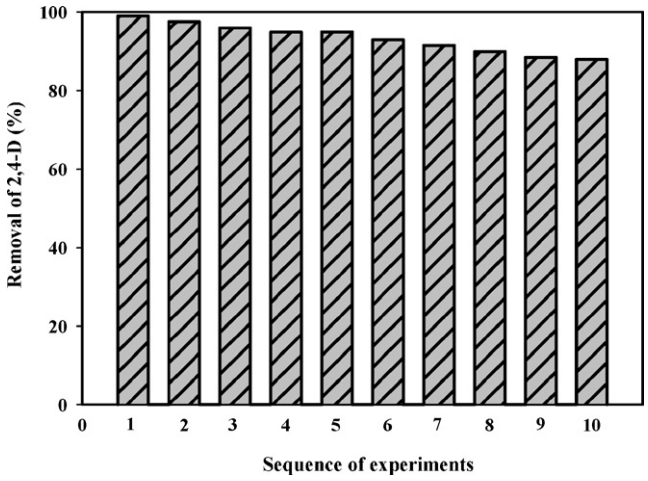

Fig. 10. The evaluation of the $CuInS_2$–TiO_2 NT catalyst stability.

3.10. Stability of the $CuInS_2$–TiO_2 NT

The stability and reuse of the photocatalyst are of great importance in the photodegradation of organic pollutants. To evaluate the stability of the $CuInS_2$–TiO_2 NT catalyst, the photoelectrocatalytic degradation ability of the catalyst was investigated by repeating the photocatalytical degradation of 2,4-D for 10 times. The $CuInS_2$–TiO_2 NT was cleaned for 30 min with ultrasonication after each experiment. Fig. 10 shows that the removal efficiency of 2,4-D remained as high as 90% when the catalyst was used for 10 times. This indicates that the $CuInS_2$–TiO_2 NT catalyst has excellent photoelectrochemical stability during the photoelectrocatalytic process.

4. Conclusions

A new $CuInS_2$–TiO_2 NT catalyst was prepared by pulse electrodeposition of $CuInS_2$ NPs onto TiO_2 NT arrays. Compared with the unmodified TiO_2 NT, the $CuInS_2$–TiO_2 NT composites showed

remarkably increased photocurrent density, and thus significantly enhanced photocatalytic activity in the degradation of 2,4-D. Moreover, the $CuInS_2$–TiO_2 NT catalyst exhibited excellent photoelectrochemical stability during the PEC process, indicating a promising application in practical systems.

Acknowledgments

This work was supported by Hunan Province Natural Science Foundation of China (No. 09JJ3027), the National Basic Research Program of China (No. 2009CB421601), the National Science Foundation for Distinguished Young Scholars (No. 50725825), and the National Science Foundation of China (No. 51078129).

References

[1] H. Yang, K. Zhang, R.R. Shi, X.W. Li, X.D. Dong, Y.M. Yu, J. Alloys Compd. 413 (2006) 302–306.
[2] Y. Tao, C.Y. Wu, D.W. Mazyck, Ind. Eng. Chem. Res. 45 (2006) 5110–5116.
[3] J. Peller, O. Wiest, P.V. Kamat, Environ. Sci. Technol. 37 (2003) 1926–1932.
[4] C. Wang, D.W. Bahnemann, J.K. Dohrmann, Chem. Commun. 165 (2000) 1539–1540.
[5] N. Lu, S. Chen, H.T. Wang, X. Quan, H.M. Zhao, J. Solid State Chem. 181 (2008) 2852–2858.
[6] M.H. Zhao, Y. Chen, X. Quan, X.L. Ruan, Chin. Sci. Bull. 52 (11) (2007) 1456–1461.
[7] F. Lin, D.M. Jiang, X.M. Ma, J. Alloys Compd. 470 (2009) 375–378.
[8] Y.F. Tu, S.Y. Huang, J.P. Sang, X.W. Zou, J. Alloys Compd. 482 (2009) 382–387.
[9] K. Shankar, K.C. Tep, G.K. Mor, C.A. Grimes, J. Phys. D-Appl. Phys. 39 (2006) 2361–2366.
[10] H. Yang, C.X. Pan, J. Alloys Compd. 501 (2010) L8–L11.
[11] L.X. Yang, D.M. He, Q.Y. Cai, C.A. Grimes, J. Phys. Chem. C 111 (2007) 8214–8217.
[12] C. Encarnación-Gómeza, J.R. Vargas-Garcíaa, J.A. Toledo-Antonio, M.A. Cortes-Jacome, C. Ángeles-Chávez, J. Alloys Compd. 495 (2010) 458–461.
[13] J.G. Yu, G.P. Dai, B.B. Huang, J. Phys. Chem. C 113 (2009) 16394–16401.
[14] Y. Hou, X.Y. Li, X.J. Zou, X. Quan, G.H. Chen, Environ. Sci. Technol. 43 (2009) 858–863.
[15] A.N. Tiwari, D.K. Pandya, K.L. Chopra, Solar Cells 22 (1987) 263–273.
[16] L.Y. Sun, L.L. Kazmerski, A.H. Clark, P.J. Ireland, D.W. Morton, J. Vac. Sci. Technol. 15 (1978) 265–268.
[17] S.J. Peng, F.Y. Cheng, J. Liang, Z.L. Tao, J. Chen, J. Alloys Compd. 481 (2009) 786–791.
[18] S.Z. Kang, Y.K. Yang, W.B. Bu, J. Mu, J. Solid State Chem. 182 (2009) 2972–2976.
[19] G.K. Padam, S. Rao, Sol. Energy Mater. 13 (1986) 297–305.
[20] A. Gupta, A.N. Tiwari, A.S.N. Murthy, Sol. Energy Mater. 18 (1988) 1–8.
[21] Y. Ogawa, S. Uenishi, K. Tohyama, K. Ito, Sol. Energy Mater. 35 (1994) 157–163.
[22] J. Klaer, J. Bruns, R. Henninger, K. Siemer, R. Klenk, K. Ellmer, D. Braunig, Semicond. Sci. Technol. 13 (1998) 1456–1458.
[23] S.P. Grindle, C.W. Smith, S.D. Mittleman, Appl. Phys. Lett. 35 (1979) 24–27.
[24] H.Y. Ueng, H.L. Hwang, J. Phys. Chem. Solids 50 (1989) 1297–1305.
[25] S. Nakamura, A. Yamamoto, Sol. Energy Mater. 49 (1997) 415–421.
[26] R.N. Bhattacharya, D. Cahen, G. Hoders, Sol. Energy Mater. 10 (1984) 41–45.
[27] S.S. Kim, S.I. Na, J. Jo, D.Y. Kim, Y.C. Nah, Appl. Phys. Lett. 93 (2008) 073307–073310.
[28] C. Coutanceau, A.F. Rakotondrainibé, A. Lima, E. Garnier, S. Pronier, J.-M. Léger, C. Lamy, J. Appl. Electrochem. 34 (2004) 61–66.
[29] L.X. Yang, Q.Y. Cai, Inorg. Chem. 45 (2006) 9616–9618.
[30] Q.Y. Cai, M. Paulose, O.K. Varghese, J. Mater. Res. 20 (2005) 230–234.
[31] D.W. Bahnemann, R. Dillert, P.K.J. Robertson, in: A.I. Kokorin, D.W. Bahnemann (Eds.), Photocatalysis, VSP BS, Eindhoven, The Netherlands, 2003 (Chapter 7).
[32] K. Vinodgopal, S. Hotchandani, P.V. Kamat, J. Phys. Chem. 97 (1993) 9040–9044.
[33] H. Yamashita, Y. Ichihashi, S.G. Zhang, Y. Matrumura, Y. Souma, T. Tatsumi, M. Anpo, Appl. Surf. Sci. 305 (1997) 121–122.
[34] D.F. Ollis, Environ. Sci. Technol. 19 (6) (1985) 480–484.
[35] K. Okamoto, Y. Yamamoto, H. Tanaka, M. Hanaka, A. Itaya, Bull. Chem. Soc. Japan 58 (1985) 2023–2028.
[36] X.Z. Li, F.B. Li, C.M. Fan, Y.P. Sun, Water Res. 36 (2001) 2215–2224.
[37] M. Hepel, J. Luo, Electrochim. Acta 47 (2001) 729–740.
[38] K. Okamoto, Y. Yamamoto, H. Tanaka, M. Hanaka, A. Itaya, Bull. Chem. Soc. Japan 58 (1985) 2015–2022.
[39] X. Quan, S. Chen, J. Su, J.W. Chen, G.H. Chen, Sep. Purif. Technol. 34 (2004) 73–79.
[40] J.D. Rodgers, N.J. Bunc, Environ. Sci. Technol. 35 (2) (2001) 406–410.
[41] I. Kaiser, K. Ernst, Ch.-H. Fischer, R. Konenkamp, C. Rost, I. Sieber, M.Ch. Lux-Steiner, Sol. Energy Mater. 67 (2001) 89–96.